NASA GRANT NCC2-5070

COMPUTATION OF LIFTING WING-FLAP CONFIGURATIONS

Final Report submitted to the
NASA Ames Research Center
Moffett Field, CA 94035

Funding Dates: July 1, 1994 to June 30, 1995

University Investigator
Brian Cantwell
Department of Aeronautics and Astronautics
Stanford University, Stanford, CA 94305

NASA-Ames Investigator
Dochan Kwak
Computational Algorithms and Applications Branch
Mail Stop T27B1, NASA Ames Research Center
Moffett Field, CA 94035-1000

October 1996

1. SUMMARY

Research has been carried out on the computation of lifting wing-flap configurations. The long term goal of the research is to develop improved computational tools for the analysis and design of high lift systems. Results show that state-of-the-art computational methods are sufficient to predict time - averaged lift and overall flow field characteristics on simple high-lift configurations. Recently there has been an increased interest in the problem of airframe generated noise and experiments carried out in the 7 x 10 wind tunnel at NASA Ames have identified the flap edge as an important source of noise. A follow-on set of experiments will be conducted toward the end of 1995. The computations being carried out under this project are coordinated with these experiments. In particular, the model geometry being used in the computations is the same as that in the experiments. The geometry consists of a NACA 63-215 Mod B airfoil section which spans the 7x10 tunnel. The wing is unswept and has an aspect ratio of two. A 30% chord Fowler flap is deployed Modifications of the flap edge geometry have been shown to be effective in reducing noise and the existing code is currently being used to compute the effect of a modified geometry on the edge flow.

2. DISCUSSION

The majority of the work done under this grant has been focused on the time-averaged flow over the half-span flap configuration. Issues such as strategies for gridding the geometry were considered first. Averaged pressure distributions and flow patterns from these computations were then compared with experimental results. The agreement was very good and the current grid approaches are considered adequate for resolving the averaged flow. Next, a flap edge modification, which worked very well in the experiment, was computationally examined. For the different shape of the tip, a modification to the grid approach was needed, and this case is currently being studied. A preliminary look at the unsteady flow over the wing was also performed. The grid that gave the best results for the time-averaged case was used for this investigation. The large scale unsteadiness of the flow was resolved, but the resolution was not adequate when looking at fluctuations at acoustic scales. It was decided that a methodical approach on a 2-D model problem was needed to study the resolution issues for computing the acoustic character of this wing since unsteady computations over a complex geometry are very expensive.

3. MODELING ISSUES FOR HIGH LIFT CFD

The attached report by Mathias and Cantwell provides additional details of the work which was accomplished under this grant.

MODELLING ISSUES FOR HIGH-LIFT CFD

Donovan L. Mathias and Brian J. Cantwell
Stanford University, Stanford, California

Abstract

A three-dimensional high-lift system was computationally simulated to investigate the effect of grid topologies and turbulence modelling on the resulting solution. Four grid strategies and two turbulence models were used. The approaches were evaluated by comparing the results with experimental data and by looking at the resolved flow features. The grids differed in two areas; the flap tip and cove end region. No change in the solution was seen with different cove end treatments, but the flap modelling changed the flow character near the flap tip. Flap tip grids which wrapped around the end of the flap resolved the flow features best, but the less detailed representations were adequate for resolving the general character of the flow. Results obtained using the Spalart-Allmaras turbulence model consistently generated more lift than those obtained using the Baldwin-Barth model.

Introduction

Community noise is becomming an increasingly important issue to airplane designers as more stringent noise regulations appear imminent. As aircraft engines become much quieter, the component of noise generated by the airframe can no longer be ignored. This is particularly true because the airplane is "dirty" (i.e. high-lift sytems and landing gear deployed) when flying low enough to be heard by the community. For example, during a landing approach the engines are typically at a reduced power setting, while the flaps are deflected the maximum amount possible. For this reason, high-lift system acoustics is important to the overall noise generated by an aircraft.

A major component of high-lift noise is attributed to the flow at the tip of the flap. The mean flow in this region has been computationally and experimentally studied by several investigators.[1-4] Much has been learned as a result of this work, as the two approaches have produced results that agree nicely. However, as the flow is examined in greater detail, it is unclear what additional issues will arise. Certainly from the computational point of view, additional resolution will be necessary to have any hope of capturing information on the scales that are important to the acoustics of the flow. Due to the finite computer resources, the refinement of the meshes must be done carefully so that the number of grid points remains manageble while resolving the key flow features. In addition, the fine details of the flow become very sensitive to additional parameters such as the turbulence model. All of these issues must be addressed for there to be a realistic hope of computationally gaining insight into the acoustics of the high-lift system.

The present study deals with two of the issues that promise to play an important role in computing high-lift flows, namely the grid topology and the turbulence model. Several grid schemes have been suggested for high-lift systems.[1-3,5] The basic difference between the approaches occurs at the flap tip and at the junction between the flapped and unflapped portion of the main element. An evaluation of the approaches is useful before real resolution studies are performed. Also, two turbulence models are commonly used for high-lift flows; the model developed by Baldwin and Barth[6] and a more recent model of Spallart and Allmaras.[7] A comparison of these two models will also prove useful for future work.

This paper contains computed results for four grid topologies and two turbulence models applied to a simple high-lift configuration. The geometry first studied in Ref.[1] is used for this study because it contains the key ingredients of a high-lift system while remaining basic enough to compute without further obscuring the important regions of the flow (Figure 1). The wing was positioned inside a wind tunnel test section at an angle of attack of ten degrees. The flap was deflected 39° from the stowed location, and when deployed overlapped the main element by 0.026 chords. The vertical gap between the lower surface of the main element and the highest position on the top of the flap was 0.017 chords.

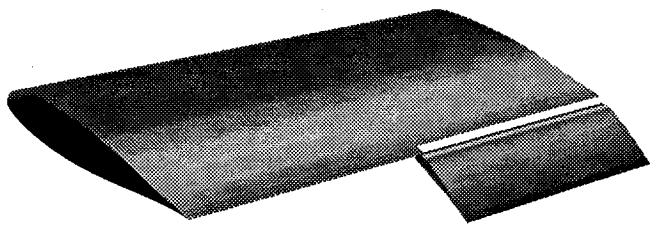

Fig. 1 High-lift system studied.

Also, quality experimental data is available for this configuration.[4] The primary means of evaluation of the parameters in this study is comparison of computed lift and pressure distributions with the experimental results. A brief discussion of the flow structure is also included. All of the computed results were obtained using the steady-state equations, and the experimental data has been time averaged for comparative purposes.

Computational Grids

Structured, overset grids were used to model the geometry in all cases, similar to the approach used in Refs. [1-3] The basic grid remains the same in the four topologies studied, with the treatment of the flap tip and end of the cove region being the difference. The wing surfaces are modeled using C-H grids, with the inner boundary of the C wrapping around the wing in the streamwise direction. The C's are copied into a spanwise "stack" to form a three-dimensional grid zone. This approach was employed for the flap and main wing elements. The main element was built of two zones: the flapped and unflapped portion each required individual zones. A rectangular H-H grid was used to model the wind tunnel test section. Final grid dimensions for the unflapped main element, flapped main element, flap, and wind tunnel section were 185x40x52, 227x40x80, 155x40x59, and 85x40x30 respectively. The individual zones were merged using the PEGSUS code.[8] Wall spacing for all wing elements was 10^{-5} chords, resulting in an average y^+ of approximately one. An inviscid test section was modeled, so the wall spacing for the wing tunnel zone was much larger.

The first topology studied, referred to as mesh A, consisted only of the four zones previously described: no zones were included to explicitly model the cove end and flap tip. Instead, boundary conditions were specified to create solid surfaces using points in the existing zones. This is the approach used in Ref. [5] to study a similar geometry. The details of the flow in these regions were not expected to be seen, but this topology shows how edge models change the flow in the rest of the flowfield. Figure 2 illustrates how the points in the flapped main element zone are used to represent the flap edge. Points in the wake, which are positioned at the proper spanwise location, are given a no-slip boundary condition. The effective flap tip is the region within the outline of the flap surface in Fig. 2, a course representation results, since the main element grid is not designed to resolve this portion of the flow. The end of the cove, at the junction between the flapped and unflapped main element sections, is treated in the same fashion. Points in the flapped main element zone are used as no-slip points on the end surface. Figure 3 shows the resulting representation. This region is expected to be resolved more completely than the flap tip, because the mail element zone contains a fair number of points in this vicinity.

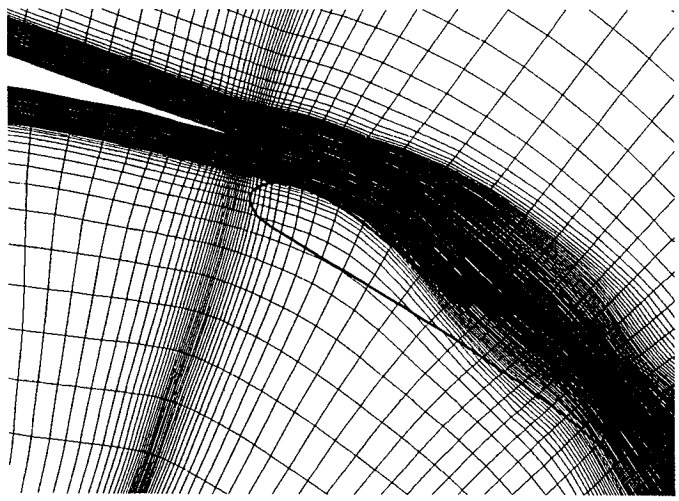

Fig. 2 Mesh A flap tip representation.

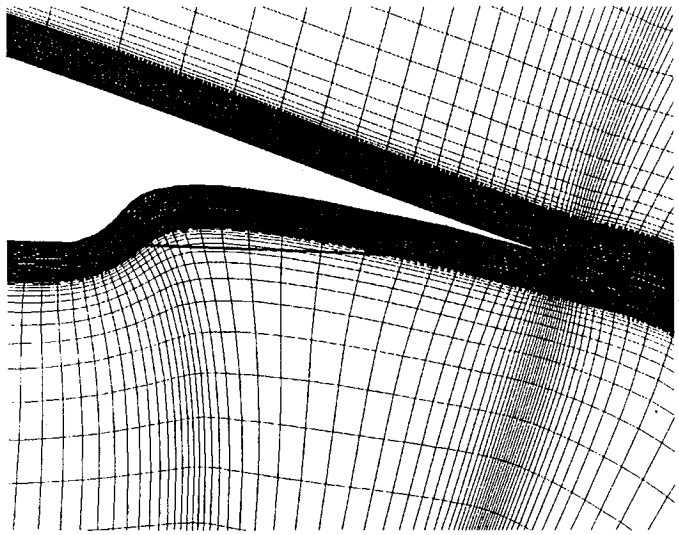

Fig. 3 Mesh A cove end representation.

Mesh B is identical to mesh A, except a grid zone is added to model the flap tip (Fig. 4). The new zone is an O-H grid which wraps around the tip of the flap onto the flap surface as shown in Fig. 4. This zone is created by algebraically generating the portion of the grid that represents the flap tip. The mesh is then hyperbolically grown onto the surface using the SURGRID[9] program. Once the surface grid is made, HYPGEN[10] is used to fill in the volume grid. This zone contains 77x57x57 points in the streamwise, spanwise and normal directions.

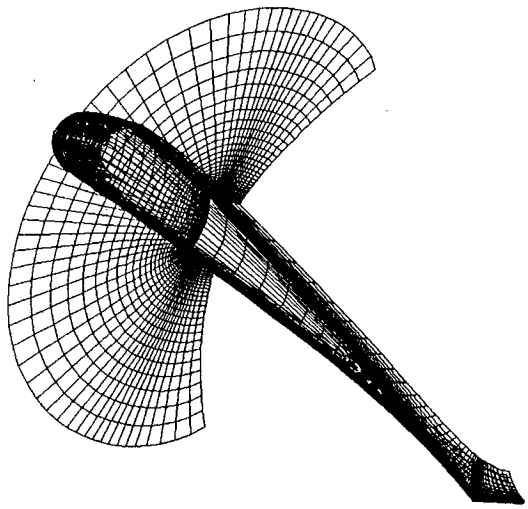

Fig. 4 Mesh B flap tip grid.

To create mesh C, an H-H zone that models the cove end was added to the previous topology. A spanwise station of the new zone is shown in Fig. 5. The outer boundary of this zone was conformed to the shape of the cove end. Individual planes were then copied in the spanwise direction. This zone was created to position points near the edges of the main element surfaces, as opposed to the course representaion of this surface in meshes A and B. The points previously used to model the solid wall were left in place, but the no-slip boundary condition was no longer prescribed. Instead, the points were updated by interpolation from the new zone.

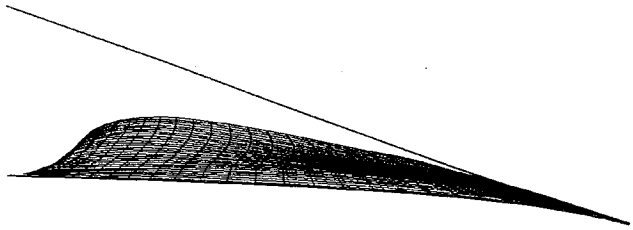

Fig. 5 Mesh C cove end grid.

In the fourth topology, mesh D, the O-H flap tip zone is replaced by an H-H zone. This mesh is nearly identical to the one used in Refs. [1-3] with slightly more points on the flap surface. The flap tip grid was first created as a two-dimensional plane, as shown in Fig. 6. The plane was generated so that grid lines would follow the upper and lower surfaces, as well as the leading and trailing edges. The surface of the flap fell a few grid cells from the outer boundary of this zone so that overlap between the zones was maintained. When the planes were copied to fill in the third dimension, a few planes had to be placed inside the flap surface. If the first tip grid plane was positioned directly on the flap tip surface, convergence problems were experienced.[1] By moving the first plane within the flap, strong flow gradients were moved to the interior of the flap tip grid, allowing the solution to converge.

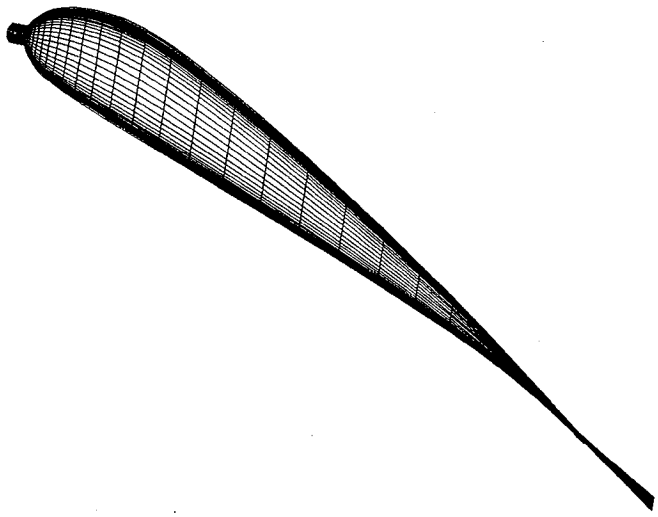

Fig. 6 Mesh D flap tip grid.

Results and Discussion

All of the computed results were obtained using the incompressible Navier-Stokes flow solver INS3D-UP.[11] INS3D-UP has given accurate results for high-lift investigations in the past.[3] The experimental data was collected at a free stream Mach number of 0.22[4] which allows an incompressible code to be used. It was felt that any compressibility would be restricted to small regions and would not have a measureable effect on the overall flow. Any loss of accuracy was offset by the rapid convergence of the incompressible solver, requiring approximately 450 iterations and 20 Cray C-90 hours per case. All of the grids were run using the Baldwin-Barth turbulence model. No modelling of boundary layer transition was implemented resulting in fully turbulent runs. To evaluate differences between models, mesh C was also computed using the model of Spalart and Allmaras. Convergence was approximately the same for all the meshes despite the difference in total grid points.

When comparing the computed results, no discernable difference in pressure or lift distributions between meshes B and C. Any differences between the meshes would certainly start in the vicinity of the cove end. Figure 7 shows the computed pressure distributions at the cove end for meshes B and C. The two curves are coincident over the entire plot. Other regions are not shown, but this trend holds at every station examined. Therefore, we conclude that the addition of the cove end zone had virtually no influence on the solution. Because the flapped main element grid contained many points near the junction of the flapped and unflapped sections, the flow was well resolved without the additional zone. Cove regions tend to be fairly shallow, so the fine normal spacing on the main element resulted in many points in this region. Also, the spanwise spacing was fine in this reion so that adequate overlap between the two main element zones was maintained. It appears that by resolving the flow on the main element, the cove region is automatically taken care of in this case. For the rest of this discussion, the results for meshes B and C will be treated as a single result.

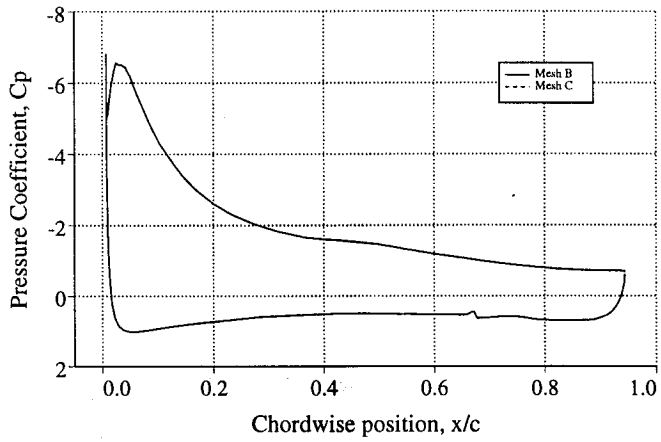

Fig. 7 Pressure distribution comparison for meshes B and C at wing mid-span.

Table 1 contains a comparison of the total integrated lift coefficient for all the computed cases as well as the experimental result. The lowest lift coefficient computed was for mesh A (C_L=2.295), while the highest occured for mesh C with the Sapllart-Allmaras turbulence model (C_L=2.332). Meshes B/C and D fell between these values. The experimental value of C_L=2.216 is lower than the computed results for all cases. This comparison suggests that mesh A, with the lowest amount of resolution, would be the topology of choice for computing C_L. Of course, this was not the expected as more precise treatment of the mesh generally is condsidered more desirable. By looking at other means of comparison, it becomes clear that mesh A does would not necessarily be the best choice for all cases. However, this result does suggest that neglecting the flap edge and cove end is reasonable for a rudimentary simulation. It also becomes apparent that the choice of turbulence models does play a signifigant role in the computations, even on the relatively large scale results such as C_L. Changing only the turbulence model caused the lift coefficient to increase from 2.303 to 2.332, a difference of 1.3%. This does not seem like a big change until this is compared with the changes do to grid modification, which changed C_L by only 0.3%. Mesh A's C_L differs from the experimental value by 3.6%, while the mesh C plus Sapllart-Allmaras model misses by 5.2%. As mentioned, though, this comparison is only one means of evaluating the issues at hand.

Table 1 Total lift coefficient comparison.

Configuration	*CL*
Mesh A	2.295
Mesh B/C	2.303
Mesh D	2.000
Mesh C + S-A turb. model	2.332
Experiment	2.216

Perhaps more information is contained in the lift distributions. Figure 8 contains a plot of the section lift coefficient over the span of the main element for all four cases and the experiment. Meshes A and B/C agree with the experimental values near the wall on the unflapped portion of the wing. Meshes D and E are off by slightly more, but all of the computed cases differ near the wing mid-span. The agreement becomes even worse for the flapped half of the wing, where all of the computed cases are off by 0.1 in C_l. The general shape of the lift distribution is captured remarkably well in all cases.

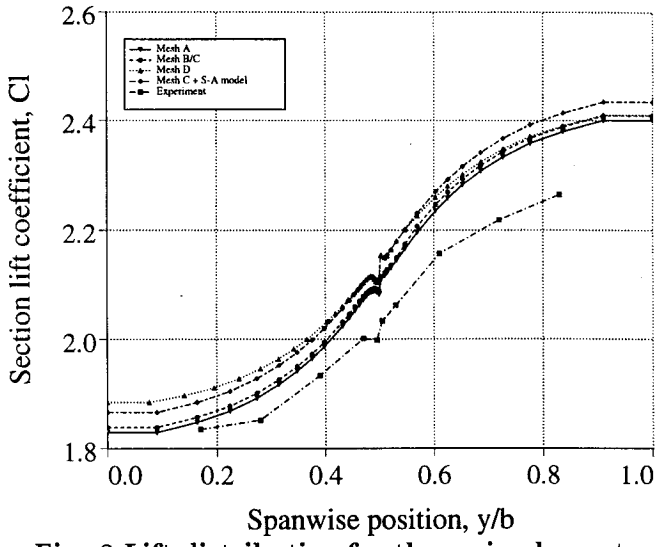

Fig. 8 Lift distribution for the main element.

Figure 9 contains a similar plot for the flap element. Again all of the computed results are higher than the experimentally measured values. Near the flap tip (y/b=0.5) the different topologies exhibit different flow features. The cases with more attention paid to resolving the flow near the edge of the flap show a lift peak in this region. This occurs because the tip vortex was captured and a high velocity was present beneath the vortex core. The lift, therefore, increases. Here is a case of the more complex topologies resolving the flow more completely, but not agreeing with the experimental data as closely. The experimental set-up did not contain enough resolution to resolve the lift peak at the flap edge. While the extra grid at the flap tip did change the character of the curve in Fig. 9, it was a local change. The curves for Meshes B/C and A become nearly a single line by y/b=0.6. This further supports the idea that less resolution is acceptable for loads calculation, for example, but to investigate the flow physics a course representation of the flap tip misses important features. As with the main element, changing from the B-B to S-A turbulence model increases the lift almost uniformly across the span.

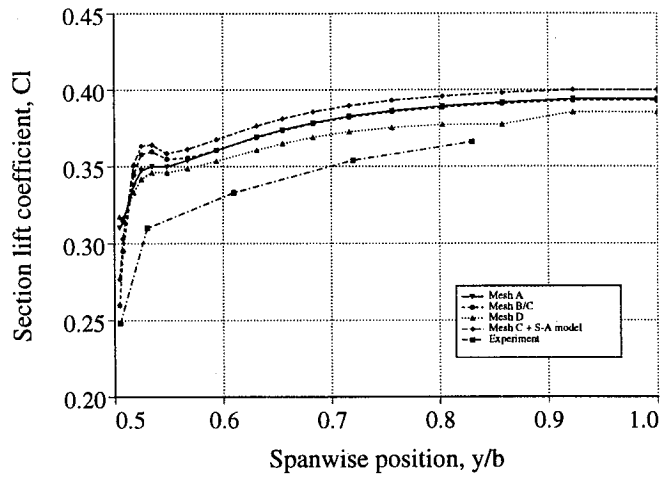

Fig. 9 Lift distribution for the flap element.

The pressure distributions for each element provide a more detailed description of the flow. Figure 10 shows a chordwise pressure distribution for the unflapped main element near the mid-span (y/b=0.498). The difference between the four computational cases is barely perceptable. All agree with the experimental results over most of the chord. The computed suction peak is slightly wider than measured experimentally, while the levels of maximum suction are about the same. Computationally there exists higher pressure coefficients over most of the lower surface of the element. The small differences in this plot are responsible for the much lower levels of C_L agreement seen in Table 1. From this figure, it is not clear that any of the grid topologies did a better job than the others.

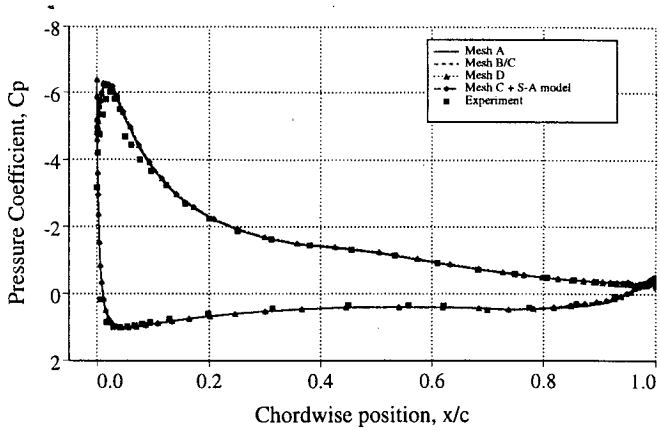

Fig. 10 Pressure distribution for the unflapped main element (y/b = 0.498).

Pressure distributions on the flapped side of the mid-span (y/b=0.502) are shown in Fig. 11. The results are nearly identical to the unflapped portion of the wing. No difference between the computed cases is evident: all agree well with the experimental data. Again, the wider computed suction peak and higher lower surface pressures are seen. Stations near the mid-span were chosen for comparison because this region contained most of the interesting flow features. If any difference was to be seen by adding the cove end grid, surely it would be seen near the cove end.

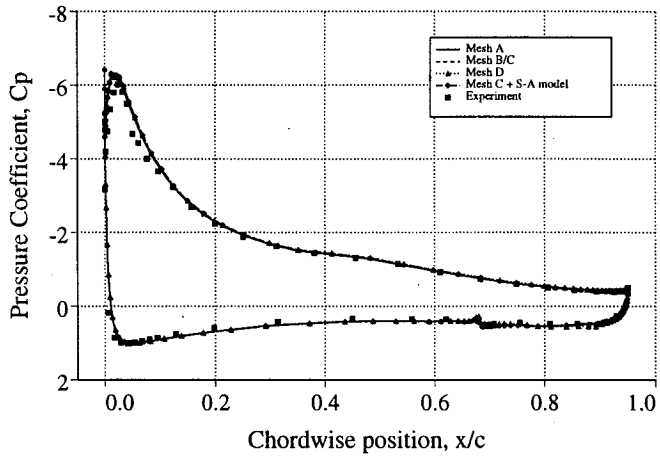

Fig. 11 Pressure distribution for the flapped main element (y/b = 0.502).

The real test of the grid schemes occurred at the tip of the flap. Figure 12 shows the pressure distributions at the flap tip (y/b=0.502). Major differences between the cases were found at this point in the flow. Mesh B/C came closest to resolving the aft suction on the upper surface of the flap caused by the presence of the tip vortex. Meshes A and D were not able to capture the vortex as well, so the suction was not as strong for these cases. Use of the S-A turbulence model increased the magnitude of the suction. All of the computational cases severely underpredicted the effect of the vortex, however. At the leading edge, the computed suction was overpredicted, with Meshes A and D differing by the most. Very little change was seen by switching turbulence models. On the lower surface, the computed pressures were also higher than the experimental values. Again, Meshes A and D were off by the greatest amount. The turbulence models showed little difference along the lower surface as well. Mesh A pressures on the lower surface appear jagged as a result of the poor treatment of this surface.

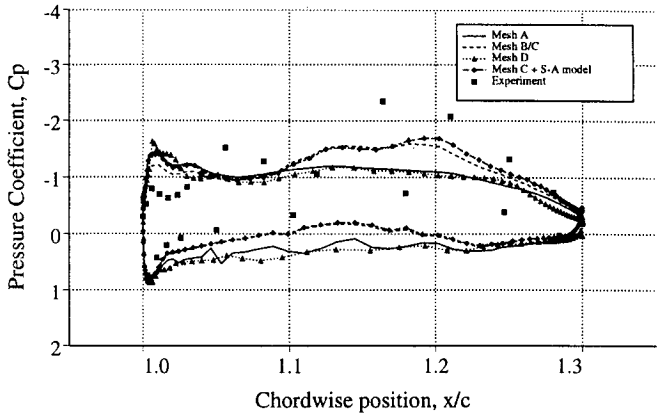

Fig. 12 Pressure distribution for the flap element (y/b = 0.502).

Figure 13 shows a similar plot slightly farther inboard of the flap tip (y/b=0.530). This figure was included to show how quickly the flow changes away from the flap tip. There is still some difference between the different cases, as well as the experimental data, but the magnitude of the disagreement has decreased dramatically. This is the reason that the simpler grid schemes did a reasonable job. When the flow becomes closely aligned with the chord, the difference between the grid schemes diminishes because the chordwise distribution of grid points was the same for all cases. The key to the difference between the meshes is really one of spanwise resolution. Meshes that wrap around the flap tip better resolve the spanwise gradients than those parallel to the flap sside edge. From this it is also obvious why so little difference was seen on the main element, as the spanwise spacing was the same.

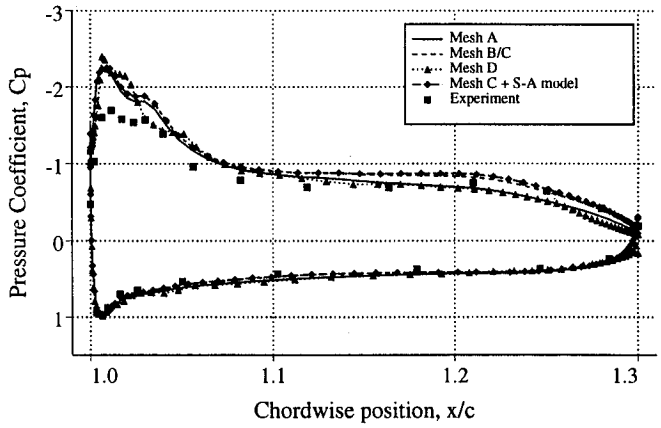

Fig. 13 Pressure distribution for the flap element (y/b = 0.530).

Figures 14 and 15 provide qualitative views of the flow for meshes A and B/C. The particle traces are colored by the local value of static pressure and are restricted to the surface of the wing. These figures show that the changes in the flow due to the different meshes are at a local level. The particle paths contained in Figs. 14 and 15 are virtually identical.

Future Work

Issues regarding comparison with the experimental data need to be further addressed. The pressure distributions generally differ by only 1-2% locally. However, when integrated to find the lift coefficient, the differences add up to increase the discrepancy by around 5%. This difference was higher than expected. Also, the fact that resolving the flow in a more realistic fashion (i.e. meshes B and C capture the tip vortex more accurately than meshes A and D) caused the agreement with the experiment to worsen was very suspicous. The experimental results that were used are from Ref. 4, but the results from previous runs differ in section lift coefficient by nearly 10%. There were protocol changes that caused this shift, but it wasn't clear which protocal was more correct at the time.

The results of this study show that topologies B and C capture more of the flow physics near the flap tip than the other approaches previously used. Therefore, the new meshes will be used to study the flow in this region to gain understanding of noise generation mechanisms and for future noise modelling efforts. Also, more detailed experimental data is needed to adress which turbulence model better resolves the details of the flow.

Conclusions

Four grid topologies and two turbulence models were used to study a simple, three-dimensional high-lift system. The simplest of the meshes (no specific treatment of the flap tip and end of the cove region) was found to be adequate for studying the large scale features of the flow, for example in a preliminary airloads study. The meshes with a flap tip grid that wrapped around the end of the flap better resolved the tip vortex than the simpler treatments. The addition of a zone to model the cove end had no influence on the solution in this case, probably due to the natural resolution of this area in the other grid zones. The flap tip grid that did not wrap around the flap tip was little better than ommitting this zone completetly. In all cases, using the Spalart-Allmaras turbulence model resulted in higher lift than the cases using the Baldwin-Barth model, everything else remaining constant. The experimental data showed that comparing integrated quantities, such as lift coefficient, did not provide an adequate criteria for judging the topologies, as the grids that best resolved the flow also differed the most with the data.

Acknowledgements

This research was funded by NASA Ames Research Center Cooperative agreement NCC 2-5070. The computing time for this work was provided by the Numerical Aerodynamics Simulation (NAS) System at NASA Ames research Center.

References

1. Mathias, D. L., "Navier-Stokes Analysis of the Flow About a Flap Edge," *Master of Science Thesis*, California Polytechnic State University, San Luis Obispo, CA, 1994.

2. Mathias, D. L., Roth, K. R., Ross, J. C., Rogers, S. E., and Cummings, R. M., "Navier-Stokes Analysis of the Flow About a Flap Edge," AIAA Paper 95-0185, Jan. 1995.

3. Mathias, D. L., Roth, K. R., Ross, J. C., Rogers, S. E., and Cummings, R. M., "Computational Investigation of a Semi-Span Flap," *Sixth International Symposium on Computational Fluid Dynamics*, Vol. II, Sept. 1995, pp. 776-781.

4. Storms, B. L. and Ross, J. C., "Aerodynamic Influence of a Finite-Span Flap on a Simple Wing," SAE Paper 95-1997, Sept. 1995.

5. Jones, K., Bideron, R., and Whitlock, M., "Application of a Navier-Stokes Solver to the Analysis of Multi-Element Airfoils and Wings Using Mulit-Zonal Grid Techniques," AIAA Paper 95-1855, June 1995.

6. Baldwin, B. S. and Barth, T. J., "A One-Equation Turbulent Transport Model for High Reynolds Number Wall Bounded Flows," AIAA Paper 91-0160, Jan. 1991.

7. Spalart, P. R. and Allmaras, S. R., "A One-Equation Turbulence Model for Aerodynamic Flows," AIAA Paper 92-0439, Jan. 1992.

8. Tramel, T. W. and Suhs, J. L., "PEGSUS 4.0 User's Manual," AEDC TR-91-8, June 1991.

9. W. M. Chan and P. G. Buning, "Surface Grid Generation Methods For Overset Grids," Computers and Fluids, Vol. 24, No. 5, pp. 509-522, 1995.

10. Chan, W. M., Ing-Tsau, C., and Buning, P. G., "User's Manual for the HYPGEN Hyperbolic Grid Generator and the HGUI Graphical User Interface," NASA TM 108791, Oct. 1993.

11. Rogers, S. E., "Numerical Solution of the Incompressible Navier-Stokes Equations," NASA TM 102199, Nov. 1990.

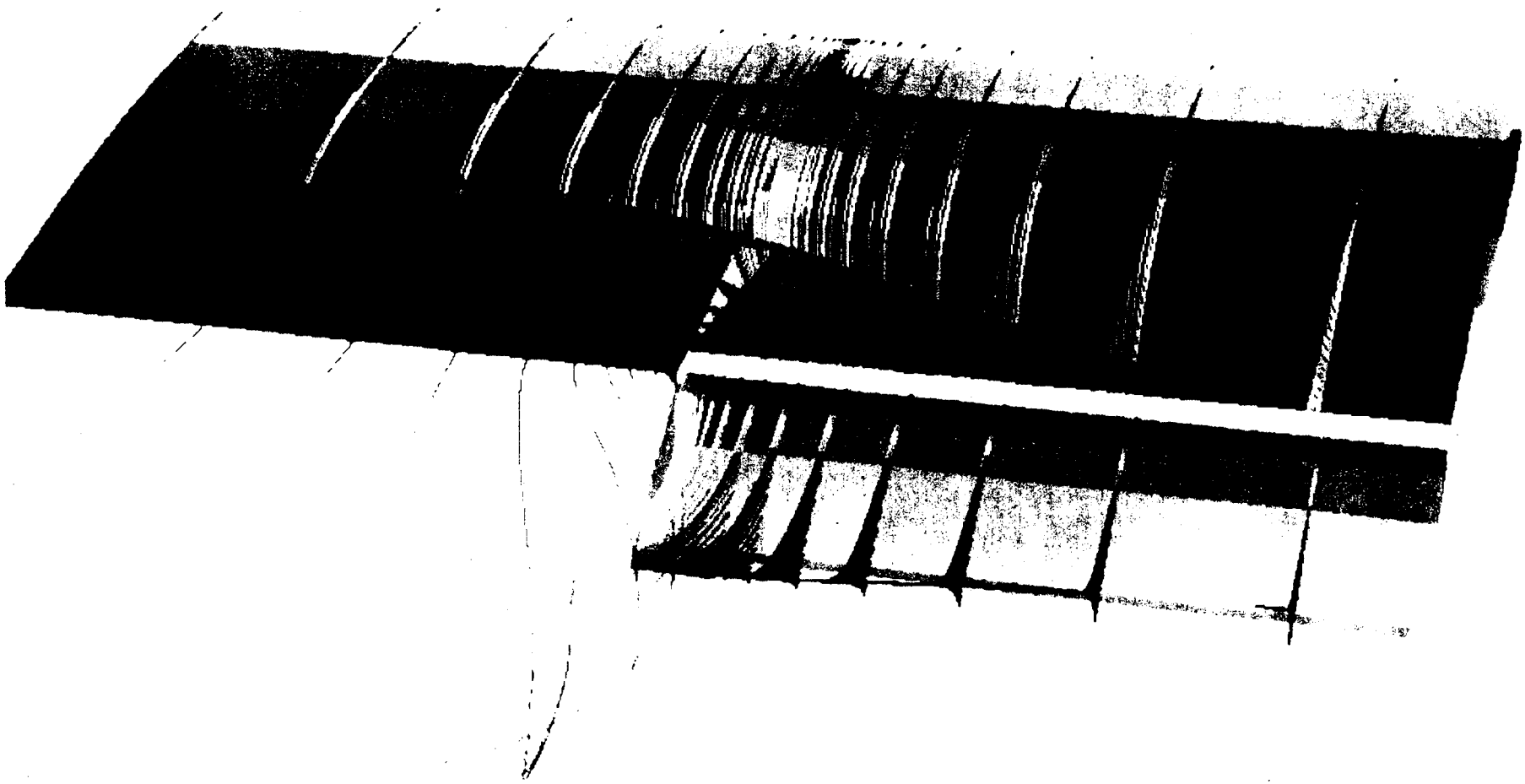

Fig. 14 Particle Traces Colored by Static Pressure for Mesh A

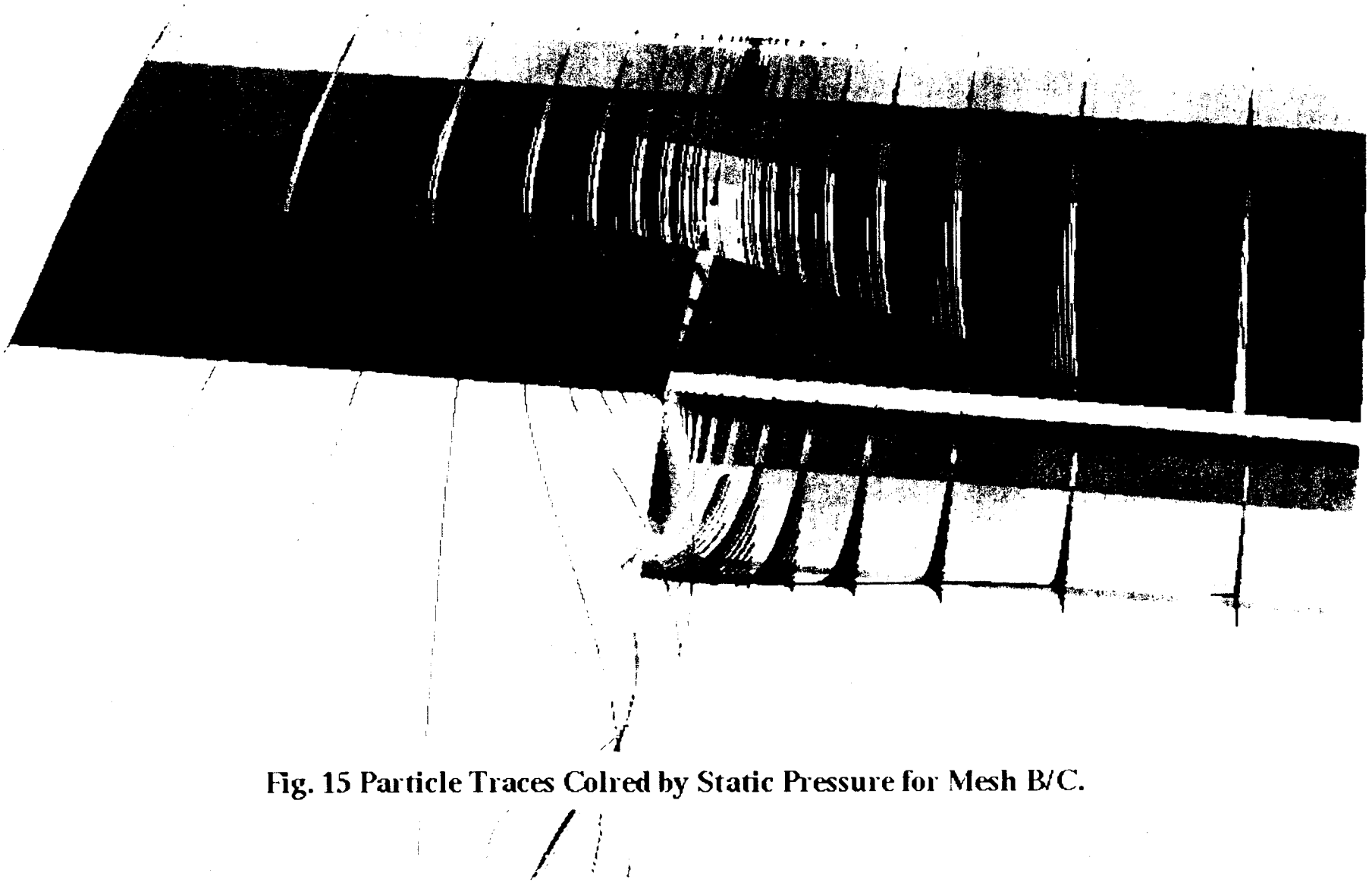

Fig. 15 Particle Traces Colred by Static Pressure for Mesh B/C.